

**Recent changes in particulate air pollution over China observed from space and the ground: Effectiveness of emission control**

*Jintai Lin, Chris Nielsen, Yu Zhao, Yu Lei, Yang Liu, Michael B. McElroy*

Pages: 36

Figures: 11

Tables: 1

## 1. Controls on emissions of aerosols and precursors

This section discusses levels of emissions of aerosols and their precursors in China for the year 2005, emission regulations implemented in recent years, and consequent estimates of emission changes from 2005 to 2010.

### 1.1 Primary PM

Large emissions of anthropogenic primary PM are a major factor in the high aerosol loadings in China. Among a variety of anthropogenic sources of PM, production of cement, combustion of coal for power generation, and burning of biofuels for residential use are estimated to be the most important contributors, comprising about 60% of total emissions of both PM<sub>10</sub> and PM<sub>2.5</sub> in 2005 (1) (Figure S1). In recent years, the government has heightened efforts to reduce emissions of primary PM from these sources.

Cement production is estimated to contribute to about 23.8% of total anthropogenic emissions of primary PM<sub>2.5</sub> and 25.7% for PM<sub>10</sub> in 2005, emitting 3.48 Tg of PM<sub>2.5</sub> and 1.99 Tg of PM larger than 2.5 μm but smaller than 10 μm (PM<sub>2.5-10</sub>) (2). In the cement industry, a new emission standard announced in 2003 has been in effect since 2004, reducing permitted levels of PM emissions by as much as 67% depending on the kiln type (3). At the same time, many small, highly-emitting shaft kilns have been replaced by larger, more efficient precalciner kilns combined with modern baghouses for PM control. Even taking into account sharp increases in cement production, the new emission standard and the shift in the industry's technology distribution are estimated to have reduced PM emissions from cement production by more than 60% from 2005 to 2010 (2),

with a much larger effect on  $PM_{2.5-10}$  as determined by the technology used for emission control (2, 4).

Similarly, a stricter PM emission standard for power plants has been in effect following its announcement in 2003 (5), and an increasing industry share of large, new, coal-fired power plants (in part due to expanded mandated early retirement of inefficient small plants during the 2006-2010 period of the Eleventh Five-Year Plan, 11<sup>th</sup> FYP) has brought greater penetration of modern electrostatic precipitators and baghouses for PM control. Also reducing PM emissions has been the requirement since 2004 that most existing and all new coal-fired power plants install flue gas desulfurization (FGD) systems (also discussed below), which have a side-benefit of washing out particles in flue gases. As a result, bottom-up estimates updated from Zhao et al. (6) indicate that PM emissions from coal-fired power plants should have declined by more than 30% from 2005 to 2010. Similar to controls in cement industry, controls are more effective for  $PM_{2.5-10}$  than for smaller particles (6).

Combustion of biofuels (such as crop wastes and wood) occurs mainly in rural areas for heating and cooking. Use of biofuels is believed to have declined in recent years as more than 100 million people have migrated from the countryside in swiftly urbanizing China and as use of processed fuels, more efficient combustion technologies, and electricity have expanded in rural areas (7). This has resulted in a reduction of PM emissions from biofuel burning. Quantifying the impact, however, is difficult due to poor data on this informal, largely non-commercial form of energy use.

Reduced emissions from these three primary sources are estimated to have resulted in an overall reduction of anthropogenic emissions of primary PM in China.

## 1.2 SO<sub>2</sub>

Anthropogenic emissions of SO<sub>2</sub> (Figure S2a) are associated mainly with combustion of coal in power plants and other heavy industry sectors. Under strong environmental pressure, the Chinese government has targeted the power sector specifically for control of emissions of SO<sub>2</sub> during the 11<sup>th</sup> FYP (2006-2010). The 11<sup>th</sup> FYP set targets for reduction both of the national energy intensity (i.e., energy consumption per unit GDP output) and of emissions of SO<sub>2</sub>, at 20% and 10%, respectively, measured in 2010 against 2005 levels. To achieve the targets, two regulations have been enforced in the power sector. First, as noted above, is the requirement that all new thermal power units and most existing ones install FGD systems. Second, small units with low energy efficiency, totaling over 59 GW, are being gradually shut down. Bottom-up emission inventories updated from Zhao et al. (6) indicate that the FGD penetration in the coal-fired power sector should have increased from 13% in 2005 to 75% by the end of 2010, and that the share of coal consumption by large units (600MW or larger) should have increased from 11% to 43% over the same period. Consistent with these trends, official data on national SO<sub>2</sub> emissions decreased by 9% from 2005 to 2008 (8), a decline that continued in 2009 according to preliminary government analysis ([http://www.mep.gov.cn/zhxx/hjyw/201001/t20100129\\_185134.htm](http://www.mep.gov.cn/zhxx/hjyw/201001/t20100129_185134.htm)). This contrasts with swift growth in the prior decade (8).

### 1.3 NO<sub>x</sub>

Emissions of NO<sub>x</sub> are estimated to have continued to rise since 2005, resulting in increases of both nitrate concentrations and the nitrate/sulfate ratio in precipitation (9). Zhang et al. (10) estimated anthropogenic emissions of NO<sub>x</sub> in China in 2005 at 19.8 Tg/yr (Figure S2b), 44% from power plants, followed by industry (26%), transportation (24%), and the residential sector (6%). Even though power generating companies have been encouraged to install low-NO<sub>x</sub> burners (LNB) in new units, the control efficiency of this technology is relatively low, around 30-40% (11). More efficient selective catalyst reduction (SCR) systems are now being deployed at newly built power units, but the penetration rate is not expected to exceed 10% by 2010. Moreover, the effectiveness of SCR for NO<sub>x</sub> control in China is currently uncertain, as the systems depend largely on the amount of ammonia used during the de-NO<sub>x</sub> process, which is difficult both to assure and to predict.

Estimated emissions of NO<sub>x</sub> from the cement industry, accounting for 6.4% of China's total in 2005, have grown significantly from 1.26 Tg in 2005 to 2.10 Tg in 2010 (2). During this period, increases in both cement production and emission factors due to replacement of shaft kilns by precalciner kilns have contributed to the increase of NO<sub>x</sub> emissions, and few control measures are available to slow this trend.

In the transportation sector, although new on-road vehicles have been required to meet Chinese Stage II and III standards (equivalent to Euro II and Euro III) in 2004 and 2007 respectively, NO<sub>x</sub> emissions are still expected to have risen by about 10% from

2005 to 2010. This is a consequence mainly of large increases in fuel consumption by China's sharply expanding national vehicle fleet (12).

#### 1.4 NMVOC

Similar to  $\text{NO}_x$ , emissions of NMVOC (Figure S2c) have not been regulated stringently (13). Anthropogenic NMVOC are emitted mainly from combustion of biofuels, transportation sources, and the production and use of industrial solvents. Under current policies, emissions from biofuel combustion (mainly in rural areas) are estimated to have declined from 4.8 Tg/yr in 2005 to 4.3 Tg/yr in 2010 as a result of urbanization (13). Emissions from the transportation sector, however, have increased from 4.8 Tg/yr to 5.7 Tg/yr over the same period, due to the expansion noted above. Emissions from industrial solvents are thought to have grown even faster, from 3.5 Tg/yr to 5.0 Tg/yr. Overall, it is estimated that anthropogenic emissions of NMVOC have increased from 19.4 Tg/yr in 2005 to 22.9 Tg/yr in 2010 (i.e., an 18% increase) (13).

#### 1.5 $\text{NH}_3$

Approximately 90% of anthropogenic emissions of  $\text{NH}_3$  in China (Figure S2d) result from the use of fertilizer and from livestock wastes. Currently there are no broadly effective measures to control emissions from these sources due to the difficulty of managing diverse agricultural activities at the range of scales applicable across China. According to official Chinese statistics, these emission sources have increased slightly in recent years (14). It is expected thus that emissions of  $\text{NH}_3$  may have increased by up to 10% from 2005 to 2010 (9).

## 2. Descriptions for atmospheric measurements

## 2.1 OMI AOD

Retrievals of AOD from OMI over the period of Oct 2004 to Dec 2009 are employed in the present study. OMI is flown onboard the National Aeronautics and Space Administration (NASA) satellite Aura passing China at around 2:00 p.m. local time. It provides data with global coverage every day with a viewing pixel of  $\sim 13 \text{ km} \times 24 \text{ km}$  at nadir and a swath of 2600 km. This study employs the daily level-3 dataset OMAEROe (available at [http://disc.sci.gsfc.nasa.gov/Aura/data-holdings/OMI/omaeroe\\_v003.shtml](http://disc.sci.gsfc.nasa.gov/Aura/data-holdings/OMI/omaeroe_v003.shtml)) with a horizontal resolution of  $0.25^\circ \text{ lat} \times 0.25^\circ \text{ long}$  based on the level-2 retrieval using the multiwavelength algorithm, OMAERO (15-16). The detailed methodology for generating the OMAEROe dataset can be found at the online readme file (17). AOD values for five wavelengths are retrieved simultaneously by the algorithm, ranging from 342.5 nm to 483.5 nm, and those at 342.5 nm and 483.5 nm are employed in this study.

Factors affecting the multiwavelength algorithm include cloud contamination, surface reflectivity, aerosol height, and aerosol properties (shape, refractive index, size, etc.) (15-16, 18). Validation of OMAERO has been discussed by Curier et al. (18), Brinkma et al. (19) and Livingston et al. (20). Curier et al. (18) found that the OMAERO data for western Europe were in good agreement with values derived from the Moderate Resolution Imaging Spectroradiometer (MODIS), with a correlation coefficient of 0.66 over land. The version of the product used here is derived using surface albedo retrieved from OMI, an update from previous versions (18-20) employing surface albedo retrieved from the Multi-angle Imaging SpectroRadiometer (MISR), and is expected to contain smaller errors associated with surface albedo (J. P. Veefkind, personal communication).

### 2.1.1 Preparation of OMI AOD data

Near deserts or during winter seasons, the algorithm for OMI AOD can occasionally yield unrealistically high values as a consequence of solar radiation reflected by sands, snow or ice. Over East China (see Figure 1a for region specifications), this complication occurred mainly in winter 2004 over southern Inner Mongolia close to the borders of Shaanxi and Shanxi Provinces (i.e., around 110°E, 40°N). To remove this influence, AOD values at 483.5 nm that are larger than a threshold of 3 were excluded from the present analysis. This procedure eliminated invalid values without affecting results from other regions (Figure S3). Similarly, an upper threshold of 5 was imposed for AOD values at 342.5 nm.

A simple smoothing procedure was imposed on the daily data to enhance the analysis of interannual trends. On each day, the final AOD value for a specific grid cell was derived as the average over its AOD value and the values of the eight closest neighboring cells. On the average, there are 75 – 200 days with valid data in each year at both wavelengths over the northeastern region of East China (more in the northern provinces and less in the south) (Figure S4).

## 2.2 MODIS AOD

The MODerate Resolution Imaging Spectroradiometer (MODIS) instruments onboard the Terra and Aqua satellites are dedicated to detect tropospheric aerosols. The present study makes use of the Deep Blue AOD at 550 nm of MODIS onboard Aqua flying ~ 10 minutes ahead of Aura. The data were taken from the daily level-3 dataset at 1° lat x 1° long for product Collection 5.1, MOD08\_D3.051 (available at

[http://gdata1.sci.gsfc.nasa.gov/daac-bin/G3/gui.cgi?instance\\_id=MODIS\\_DAILY\\_L3](http://gdata1.sci.gsfc.nasa.gov/daac-bin/G3/gui.cgi?instance_id=MODIS_DAILY_L3))

(21-23). MODIS measures aerosols with near-global coverage each day at a wide spectral range of 410-15000 nm. The algorithm to retrieve AOD over land evaluates AOD at three wavelengths (470 nm, 660 nm, and 2130 nm). AOD values at 550 nm are interpolated from 470 nm and 660 nm using the Ångström law (21). Systematic validation of MODIS AOD data was presented in previous studies (21).

The data coverage of MODIS AOD is similar to those of the OMI products. On the average, there are 75 – 250 days with valid data in each year over most of the northeastern region of East China (more in the northern provinces and less in the south) (Figure S4).

### 2.3 Mass concentrations of PM<sub>10</sub> near the surface

Daily mean mass concentrations of ground-level PM<sub>10</sub> ([PM<sub>10</sub>]) were derived using the Air Pollution Index (API) data from the Ministry of Environmental Protection (MEP) of China ([http://datacenter.mep.gov.cn/TestRunQian/air\\_dairy\\_en.jsp](http://datacenter.mep.gov.cn/TestRunQian/air_dairy_en.jsp)). The API records for previous years (2000-2006) have been used to study aerosol loadings and their impacts on meteorology in China (24-28). Here the [PM<sub>10</sub>] data were analyzed for 66 major cities in East China (see Figure 1a for region specifications), including all of the four province-level municipalities (Beijing, Tianjin, Shanghai and Chongqing), 22 provincial capitals, and 40 other major cities.

On each day, the environmental protection bureau of each city uses current Chinese criteria to calculate the API level (between 0-500) of each of three species, PM<sub>10</sub>, SO<sub>2</sub> and NO<sub>2</sub>, based on measurements of their daily mean concentrations, and then reports the

highest of these values to the public, noting to which species it refers. On days with the highest API not exceeding 50, however, the ambient air is considered to be clean and specific pollutants are not identified. The API of PM<sub>10</sub> exceeds that of the other species and was the reported value typically for more than 50% of the days during Oct 2004 – Dec 2009 for the cities included in this analysis. Here days with PM<sub>10</sub> as the reported pollutant or with clean ambient air were chosen (24-25, 27-28) to analyze the trends of [PM<sub>10</sub>]; a sensitivity test excluding clean days showed trends of [PM<sub>10</sub>] with little difference from results here. The conversion from API to [PM<sub>10</sub>] is straightforward (24-25) (Figure S5). There are six thresholds for API values corresponding to six levels of [PM<sub>10</sub>]. For instance, an API score of 100 is equivalent to a [PM<sub>10</sub>] of 150 µg/m<sup>3</sup>, the current Chinese standard for “good” air quality with respect to PM<sub>10</sub>. API values falling between two thresholds can be converted to [PM<sub>10</sub>] by linear interpolation.

#### 2.4 AOD from AERONET

The ground-based AOD data were derived from the AErosol RObotic NETwork (AERONET) used widely to validate AOD measurements from satellite instruments (21). The daily level-2 data at 440 nm from three Chinese sites (Beijing, Xianghe and Taihu) including information for at least four years since Oct 2004 were included in the present analysis (29-31). Table S1 summarizes the geographical location of the sites. For comparison with OMI AOD, the measurements were averaged over 12:30 p.m. – 3:30 p.m. local time to match the overpass time of the satellite.

#### 2.5 Tropospheric vertical column density of NO<sub>2</sub> from OMI

Monthly mean Level-3 data from Oct 2004 – Dec 2009 for tropospheric vertical column densities (VCDs) of NO<sub>2</sub> are derived for OMI at a resolution of 0.125° lat x 0.125° long by KNMI (available at [http://www.temis.nl/airpollution/no2col/no2regioomimonth\\_col3.php](http://www.temis.nl/airpollution/no2col/no2regioomimonth_col3.php)), based on the retrieved Level-2 dataset DOMINO v1.0.2 (32). Uncertainties in the Level-2 product are attributed mainly to potential errors in cloud parameters, surface albedo, and *a priori* vertical profile of NO<sub>2</sub> assumed during the retrieving process (32). The Level-2 product has been validated (33-34). In deriving the monthly mean VCDs, in order to reduce the effect of cloud contamination, only viewing pixels for days with cloud radiance fractions < 50% (i.e., cloud fraction < 15%) are included. For consistency with the OMI AOD data, the monthly NO<sub>2</sub> data have been averaged over a grid of 0.25° lat x 0.25° long.

## 2.6 Surface meteorological measurements

Measurements of a variety of meteorological parameters from 232 stations across East China (see Figure 1a for region specifications) were used to evaluate changes in weather since Oct 2004, including air temperature at 2m, precipitation, relative humidity, and wind speed. These data are freely accessible through the U.S. National Oceanic and Atmospheric Administration (NOAA) National Climate Data Centre (NCDC) (<http://www7.ncdc.noaa.gov/CDO/cdo>). Most stations provide data every 6 hours; 14 sites over the northeastern region of East China report hourly data for RH at the overpass time of OMI and MODIS, enabling an evaluation of the effect of RH on the interannual trend of satellite based AOD measurements.

## 3. Analysis of interannual trend of AOD, [PM<sub>10</sub>], and NO<sub>2</sub> VCDs

Significant daily and seasonal variations were found for AOD (both satellite- and ground-based) and [PM<sub>10</sub>] data corresponding to changes in emissions of aerosols and precursors, atmospheric lifetimes of aerosols, and meteorology. To evaluate the interannual trend, a 365-day moving average was applied to the daily data to eliminate the effect of temporal variations within a year. For the same reason, a 12-month moving average was applied to the monthly data for NO<sub>2</sub> VCDs.

A simple fit for the interannual trend was derived by linear regression on the moving averaged data for AOD and [PM<sub>10</sub>] over the first four years (Figure S6). Data since Oct 2008 were not included in the linear fit in order to exclude the effect of the recent economic downturn.

The availability of AOD data defers between seasons as a result of differences in the occurrences of clouds, snow and/or ice. This may lead to complications in the calculation of interannual trends of AOD. To test this effect, interannual trends were calculated for four sensitivity cases where AOD data in particular seasons were excluded from the analysis (Figure S7). In all cases, consistent increases in AOD were found over the northeastern region of East China, in good agreement with trends calculated based on data over the entire seasons. This suggests that the data availability has insignificant impacts on interannual trends analyzed in this study.

#### 4. Comparisons of AOD from OMI and AERONET

The OMI AOD data at 483.5 nm are evaluated using the ground-based AOD measurements from AERONET. (Analysis for OMI AOD at 342.5 nm shows similar results; and the MODIS product has been evaluated intensively with the surface dataset in

previous studies (21).) The two datasets are highly correlated at the three sites (Beijing, Xianghe and Taihu) with a day-to-day correlation coefficient of 0.64-0.82. Moreover, the interannual trends for the AERONET measurements derived using linear regression are consistent with results for OMI AOD: +0.040 per year versus +0.035 per year at Beijing, +0.024 per year versus +0.013 per year at Xianghe, and 0.086 per year versus 0.15 per year at Taihu, respectively, prior to the economic downturn.

5. Effects of changes in meteorology, dust and biogenic secondary aerosols on AOD and [PM<sub>10</sub>]

#### 5.1 Relative humidity

The AOD results from both scattering and absorption of solar radiation by aerosols in the column. The absorption is relatively independent of relative humidity (RH) and normally contributes to 20% or less to the inferred values of AOD. The scattering of solar radiation by aerosols, however, has a significant dependence on RH (35). This section evaluates the effect of changes in RH on interannual trends of AOD retrieved from OMI and MODIS.

The dependence of aerosol scattering on RH is evaluated often using the hygroscopic growth factor ( $f(RH)$ ) defined as the ratio of the aerosol scattering coefficient at a given RH to that under dry conditions (36-37). Recent studies in Beijing found  $f(RH = 80\%)$  to be  $1.63 \pm 0.19$  in summer (37) and  $1.26 \pm 0.15$  during winter (38). Other studies found  $f(RH = 80\%)$  values in the range of 1.7 – 2.0 at Lin'an in the Yangtze River Delta (YRD) (39), and  $2.04 \pm 0.28$  for urban air at Guangzhou in the Pearl River Delta (PRD) (36). A simplified formula for  $f(RH)$  was proposed by Liu et al. (36):

$$f(RH) = 1 + a(RH/100)^b$$

where parameters  $a$  and  $b$  were fitted from measurements. This formula was used here to approximate  $f(RH)$  for satellite based AOD, with parameters derived from the observations quoted above to define the plausible range of  $f(RH)$  (Figure S8). A first-order estimate for the virtual “AOD at dry condition” was conducted then by dividing the AOD values by  $f(RH)$ .

For purposes of estimating the effect of RH on changes in AOD, hourly records of RH were taken from 14 meteorological stations in the northeastern region. Given the large viewing swaths of OMI and MODIS, hourly RH data during 1:00 p.m. – 3:00 p.m. were averaged in calculating  $f(RH)$  for each site. In removing the dependence of AOD on RH, the inferred values of  $f(RH)$  were applied to the AOD data, ignoring possible effects of RH on absorptions which are not thought to be consequential. In addition, RH is measured for the atmosphere near the surface, while satellite based AOD represents the effect of aerosols over the entire vertical column. These differences, however, are not expected to have a significant impact on our trend analysis since results based on various assumptions of  $f(RH)$  were consistent, as shown below.

Changes in the resulting “AOD at dry condition” are compared with results for the original AOD (i.e., those prior to the elimination of the effect of RH) in Figure S9. In the northeastern region, changes in the original AOD averaged over the 14 meteorological stations represent well the changes in the regional mean AOD, with a general increase up to late-2008 followed by a reduction through late-2009, when changes in AOD values

reverse again. Such changes are also consistent with results for the “AOD at dry condition” under the three assumptions for  $f(RH)$ . We conclude that changes in RH are unlikely to introduce any significant errors in our inference from satellite instruments of temporal trends in AOD.

## 5.2 Other factors

Interannual trends of AOD and  $[PM_{10}]$  are relatively insensitive to variability in other meteorological parameters, as discussed below.

Precipitation washes out aerosols and reduces AOD and  $[PM_{10}]$ . No systematic interannual trend is observed in measurements of precipitation amounts since Oct 2004 (Figure S10).

Variations in surface air temperature affect the formation of secondary aerosols. Higher temperature (Figure S11) leads to larger emissions of biogenic NMVOC and thus enhanced production of biogenic secondary organic aerosols (SOAs). This effect, however, is important mainly in summertime over regions with higher vegetation densities. Analyses of interannual trends for non-summer seasons also show increases in AOD and decreases in  $[PM_{10}]$  (Figure S7b), indicating that changes in biogenic SOAs are unlikely to be a major cause of changes in aerosols.

Aerosols in source regions can be carried off by winds. Thus higher wind speed may lead to lower values for both AOD and  $[PM_{10}]$  over source regions with higher values in downwind. This, however, cannot explain the consistent trend of AOD across both source and downwind regions of aerosols (Figures 1b-d).

Changes in the stability of the boundary layer (BL) could affect the vertical distribution of aerosols, with opposite impacts on AOD and [PM<sub>10</sub>] near the surface. No evidence is found for changes in the stability of BL that would cause constant and drastic changes in aerosols throughout the years (Figures 2a,3a).

Finally, changes in meteorological conditions in springtime could affect emissions and transport of natural dust aerosols from western China. Analysis for non-spring seasons resulted in interannual trends of aerosols similar to trends calculated based on the entire seasons (Figure S7a), suggesting changes in dust aerosols unlikely to be the main cause of changes in aerosols found in this study.

## 6. GEOS-Chem simulations

Version 8-03-01 of the global chemical transport model (CTM) GEOS-Chem ([http://wiki.seas.harvard.edu/geos-chem/index.php/Main\\_Page](http://wiki.seas.harvard.edu/geos-chem/index.php/Main_Page)) was used to evaluate the net effect of changes in precursor emissions on secondary inorganic aerosols (SIOAs) (sulfate, nitrate, and ammonium) from Oct 2004 – Sep 2005 to Oct 2007 – Sep 2008 over the northeastern region of East China. This version includes an updated estimate for aerosol optical properties based on the recent work of Drury et al. (40) It was run with the full O<sub>x</sub>-NO<sub>x</sub>-CO-NMVOC chemistry with online calculations for SIOAs, dust and sea salts. Online simulation of SOAs is under significant development and is not included in this study. The model was run at a resolution of 2° lat x 2.5° long with 47 vertical layers. It was driven by the assimilated meteorological fields of GEOS-5 produced by the NASA Global Modeling and Assimilation Office (GMAO).

The base anthropogenic emissions in Asia for NO<sub>x</sub>, carbon monoxide (CO), NMVOC, SO<sub>2</sub>, BC and OC were taken from the INTEX-B mission (10). Emissions of NH<sub>3</sub> were taken from the TRACE-P campaign (41), and values in China were increased by 22% to reach the emission budget in 2005 estimated by Zhao et al. (9). Seasonal variation of emissions from residential combustion was based on Streets et al. (41). Other anthropogenic emission sources were kept constant throughout the year.

Changes in anthropogenic emissions of precursors of SIOAs are estimated as follows. The 27% increase in the retrieved VCDs of NO<sub>2</sub> from Oct 2004 – Sep 2005 to Oct 2007 – Sep 2008 was taken to be the amount of increase in emissions of NO<sub>x</sub>. Increases in emissions of NH<sub>3</sub> over 2005 – 2010 were assumed to be linear from year to year so that increases from 2005 to 2008 were estimated to be 6%. Reductions in emissions of SO<sub>2</sub> were taken to be 9% from 2005 to 2008.

Two model simulations were compared first to evaluate changes in emissions of NO<sub>x</sub> inferred from the retrieved VCDs of NO<sub>2</sub>: one for Oct 2004 – Sep 2005 and the other for Oct 2007 – Sep 2008, with changes in emissions and meteorology taken into account. For each one-year period, simulations were conducted for four months: October, January, April and July, as representative of different seasons. It was found that the simulated VCDs of NO<sub>2</sub> increased by 21% from Oct 2004 – Sep 2005 to Oct 2007 – Sep 2008, as compared to the increase by 27% retrieved from OMI. Thus increases in emissions of NO<sub>x</sub> in accordance to changes in the retrieved VCDs of NO<sub>2</sub> may be slightly larger than the amount of 27% assumed here.

To evaluate the sole effect of changes in precursor emissions on SIOAs, model simulations were conducted then for Oct 2004, Jan 2005, Apr 2005 and Jul 2005, for two

cases with and without, respectively, the inclusion of changes in precursor emissions estimated above. It was found that changes in precursor emissions resulted in a net increase in simulated total SIOAs with a 9% increase in AOD and a 12% increase in surface mass concentration. Consistent with our analysis, Zhao et al. (9) suggested that the impact of sulfur control on acid deposition from 2005 to 2010 might be negated by the increase in emissions of NO<sub>x</sub> and NH<sub>3</sub> under current policies.

**Table S1. Descriptions of the AERONET sites in East China**

| Site    | Geography                      | Data Record <sup>1</sup> | Note                                                                                                                                                                                                                    |
|---------|--------------------------------|--------------------------|-------------------------------------------------------------------------------------------------------------------------------------------------------------------------------------------------------------------------|
| Beijing | 116.38°E<br>39.98°N<br>92.0m   | Oct 2004 –<br>Mar 2008   | Located on a terrace on the roof of the Institute of Atmospheric Physics (IAP) building (30m high)                                                                                                                      |
| Xianghe | 116.96° E<br>39.75° N<br>36.0m | Oct 2004 –<br>Jul 2009   | Installed on the roof of a four-floor building of Xianghe Observatory, IAP. The site is about 60 km southeast of Beijing, and is surrounded by a small town to the east and by agricultural fields in other directions. |
| Taihu   | 120.22° E<br>31.42° N<br>20.0m | Sep 2005 –<br>Oct 2008   | Installed near the shore of the Taihu Lake. This site is located in the Yangtze River Delta.                                                                                                                            |

1. The data record represents the time with available data over the period of Oct 2004 – Dec 2009.

**Figure S1.** Spatial distributions (at  $0.5^\circ$  lat x  $0.667^\circ$  long) of anthropogenic emissions of primary PM in China for 2005 and contributions from various sources: (a)  $PM_{2.5}$  and (b)  $PM_{10}$ . Also shown in the maps are colored boundaries of the two regions as defined in Figure 1a: northeast (yellow) and the Beijing-Tianjin area (green).

**Figure S2.** Emissions of aerosol precursors. (a-d) Spatial distributions (at  $0.5^\circ$  lat x  $0.667^\circ$  long) for anthropogenic emissions of aerosol precursors in China for 2005 and (e) annual emission budgets (Tg) from 1990 to 2010. Also shown in the maps are colored boundaries of the two regions as defined in Figure 1a: northeast (yellow) and the Beijing-Tianjin area (green). In (e), annual emissions of  $SO_2$ ,  $NO_x$  and NMVOC are taken from China Environment Yearbook 1990-2008 (8), Zhang et al. (10, 42), and Wei (13), respectively.

**Figure S3.** Number of days with invalid values for OMI AOD at 483.5 nm over Oct 2004 – Dec 2009. The grey areas do not have invalid data under current criteria.

**Figure S4.** Number of days with valid AOD data in each year averaged over Oct 2004 – Sep 2009. Also shown in colored boundaries are the regions defined by Figure 1a.

**Figure S5.** Relationship between API values and  $[PM_{10}]$ . The six thresholds for API scores are highlighted with stars, including 50, 100, 200, 300, 400, 500.

**Figure S6.** Interannual trends of AOD and  $[PM_{10}]$  over Oct 2004 – Sep 2008. The trend is derived with a simple fit using linear regression. Note the middle panels show AOD trends in cities with  $[PM_{10}]$  measurements. Also shown in colored boundaries are the regions defined by Figure 1a. Grey areas do not have valid data for trend analysis. The upper panels are the same as Figures 1b-d.

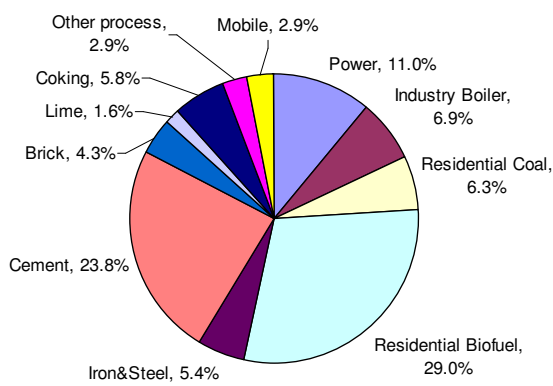
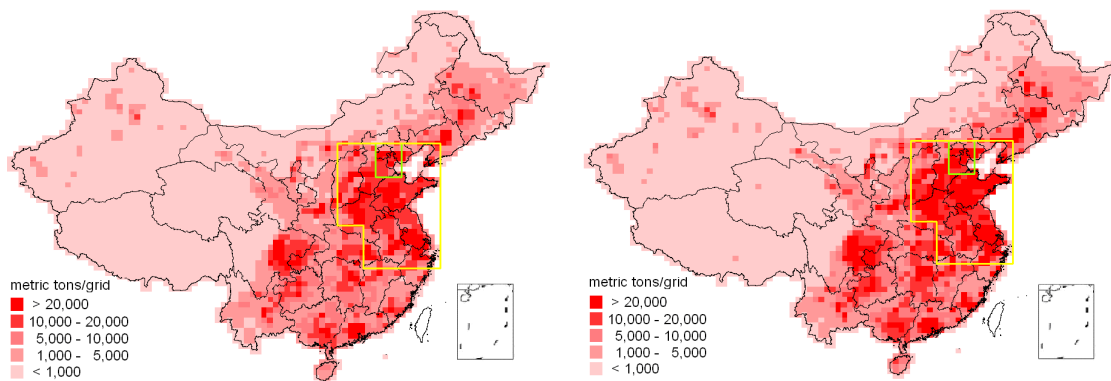
**Figure S7.** Interannual trends of OMI AOD at 483.5 nm over Oct 2004 – Sep 2008 derived with a simple fit using linear regression based on data in three out of four seasons. Also shown in colored boundaries are the regions defined by Figure 1a.

**Figure S8.** Hygroscopic growth factor ( $f(\text{RH})$ ) and its higher and lower limits. These curves are assumed in the present study for East China based on three independent studies. The curve for  $f(\text{RH}=80\%)=2.04$  is adopted from Liu et al. (36); and the other two curves are derived from measurements in Liu et al. (37) and Yan et al. (38).

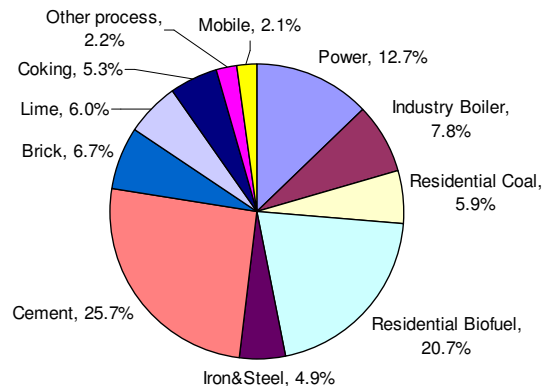
**Figure S9.** Changes in AOD values over the northeastern region of East China. Each data point represents a 365-day moving average. The black line denotes the regional mean AOD, the blue line denotes the mean AOD sampled at the 14 meteorological stations with hourly RH records, and the orange, purple and pink lines denote the “AOD at dry condition” averaged over the sites with hourly RH records assuming a  $f(\text{RH}=80\%)$  of 2.04, 1.63 and 1.26, respectively. The dashed vertical line depicts the approximate start of the Chinese economic downturn.

**Figure S10.** Measurements of precipitation over Oct 2004 – Sep 2009. Shown here are measured annual precipitation (top row) and its year-to-year variation (bottom row) at meteorological stations.

**Figure S11.** Measurements of air temperature over Oct 2004 – Sep 2009. Shown here are measured annual mean surface air temperature (top row) and its year-to-year variation (bottom row) at meteorological stations based on the 6-hourly data.

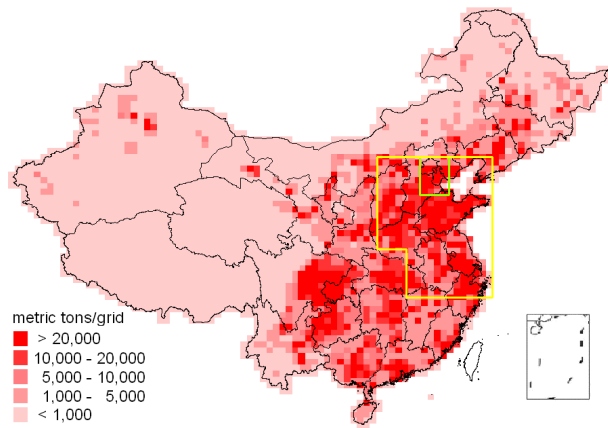


(a) PM<sub>2.5</sub>

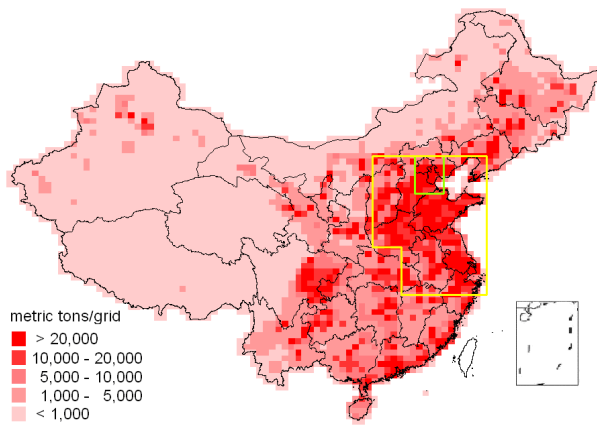


(b) PM<sub>10</sub>

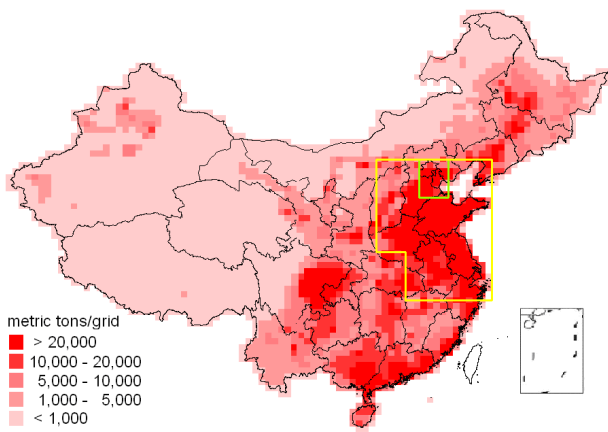
**Figure S1.**



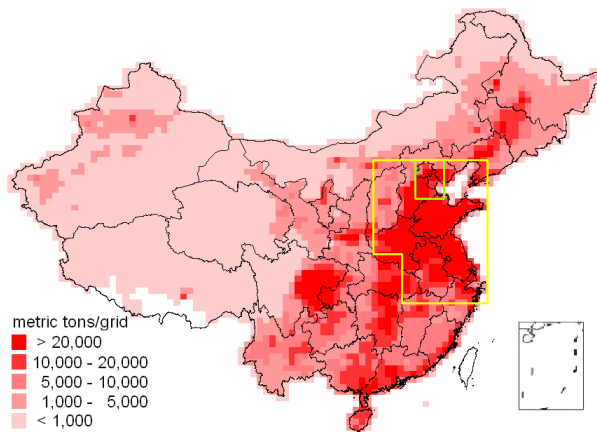
(a) SO<sub>2</sub>



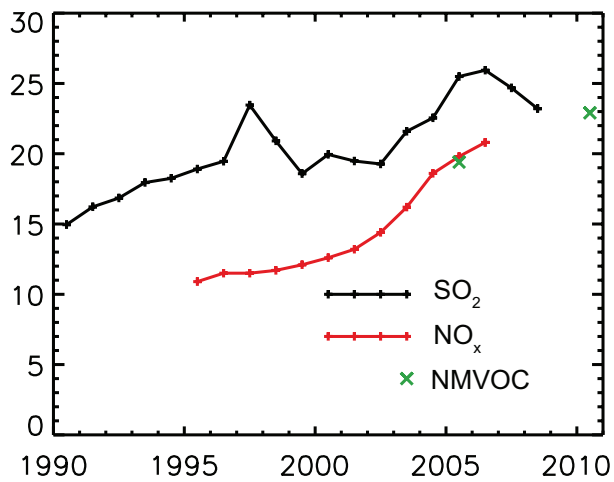
(b) NO<sub>x</sub>



(c) NMVOC



(d) NH<sub>3</sub>



(e)

**Figure S2.**

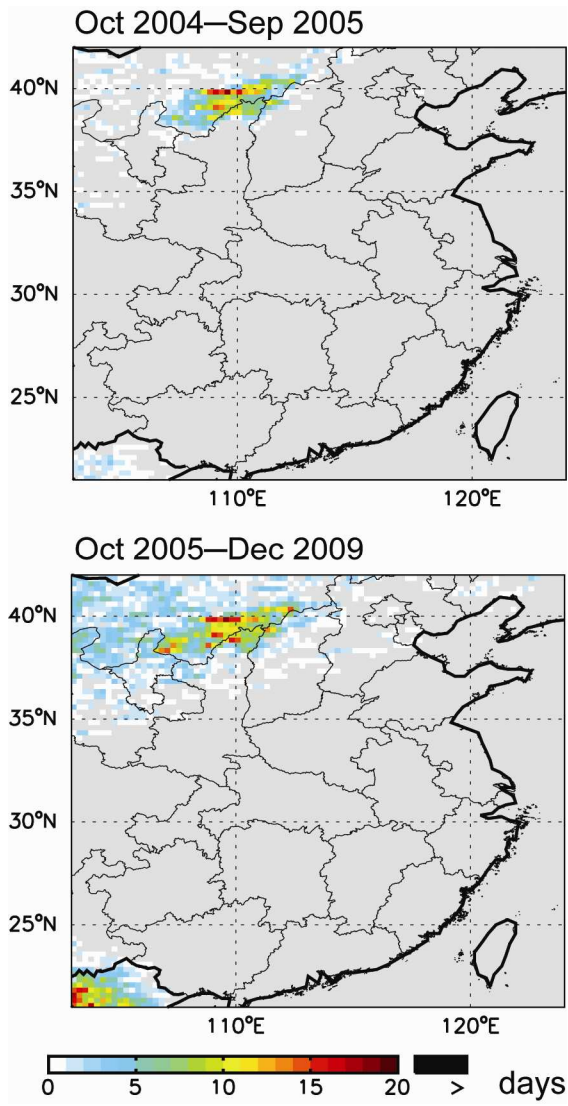


**Figure S3.**

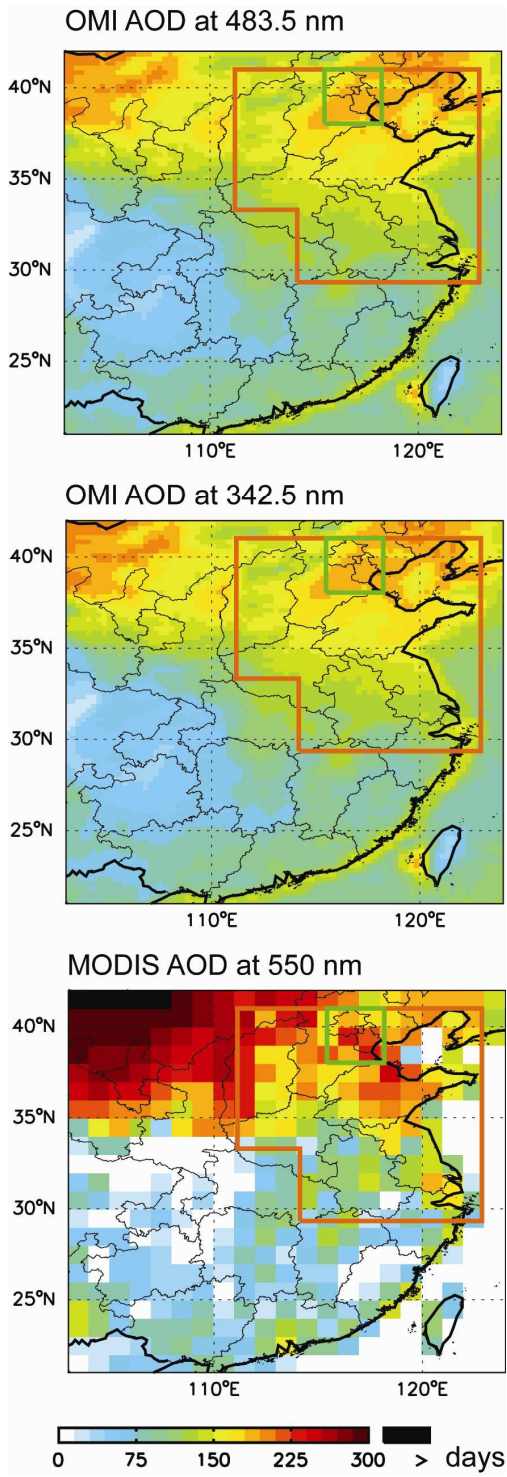


**Figure S4.**

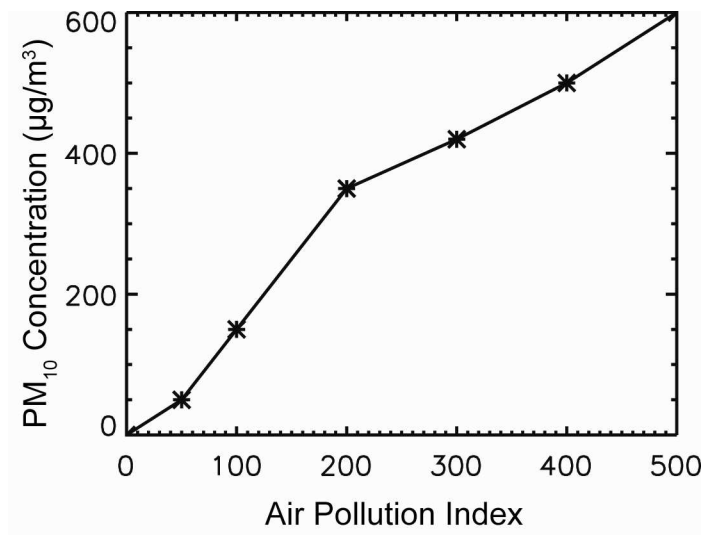


**Figure S5.**

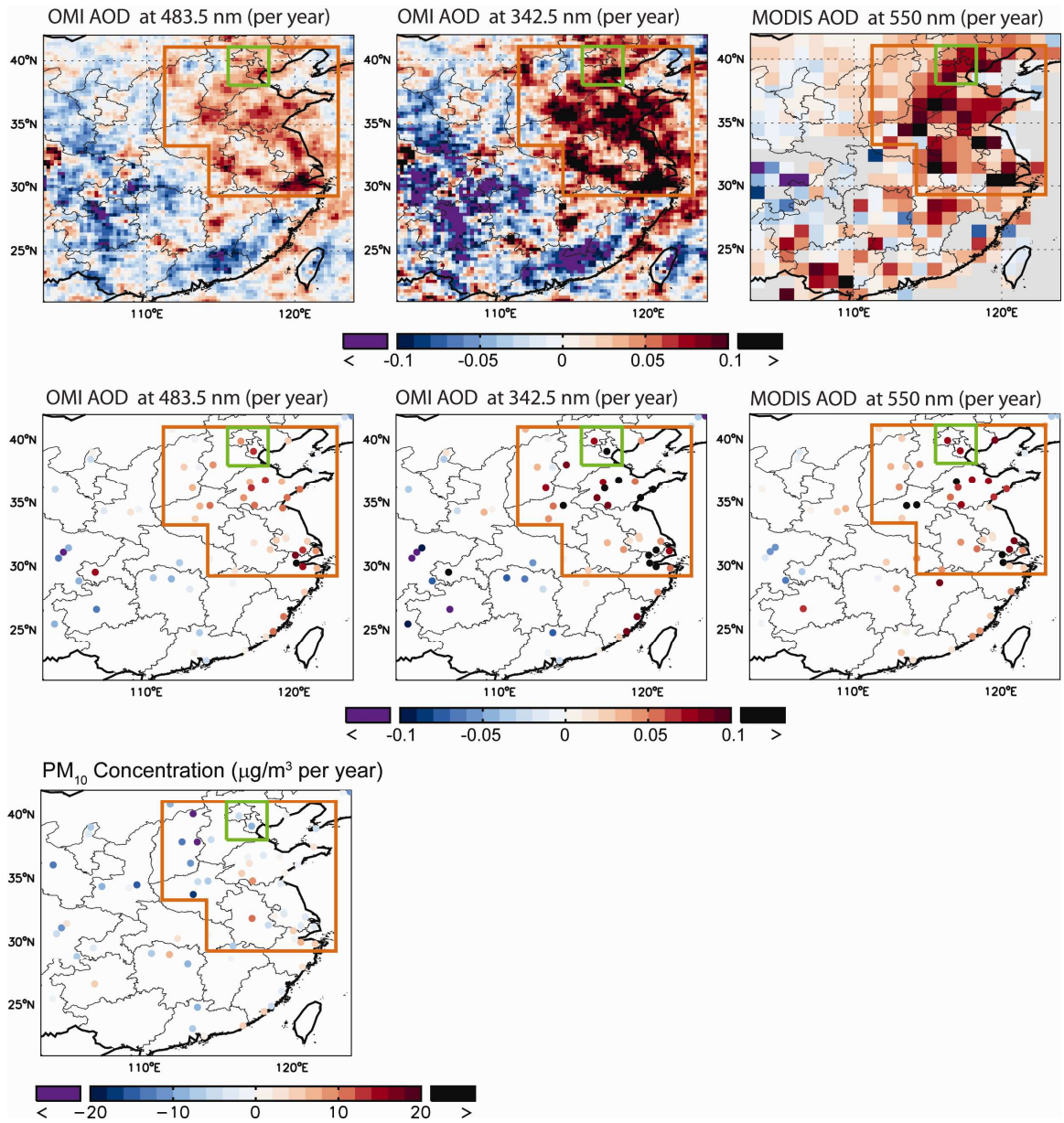


**Figure S6.**

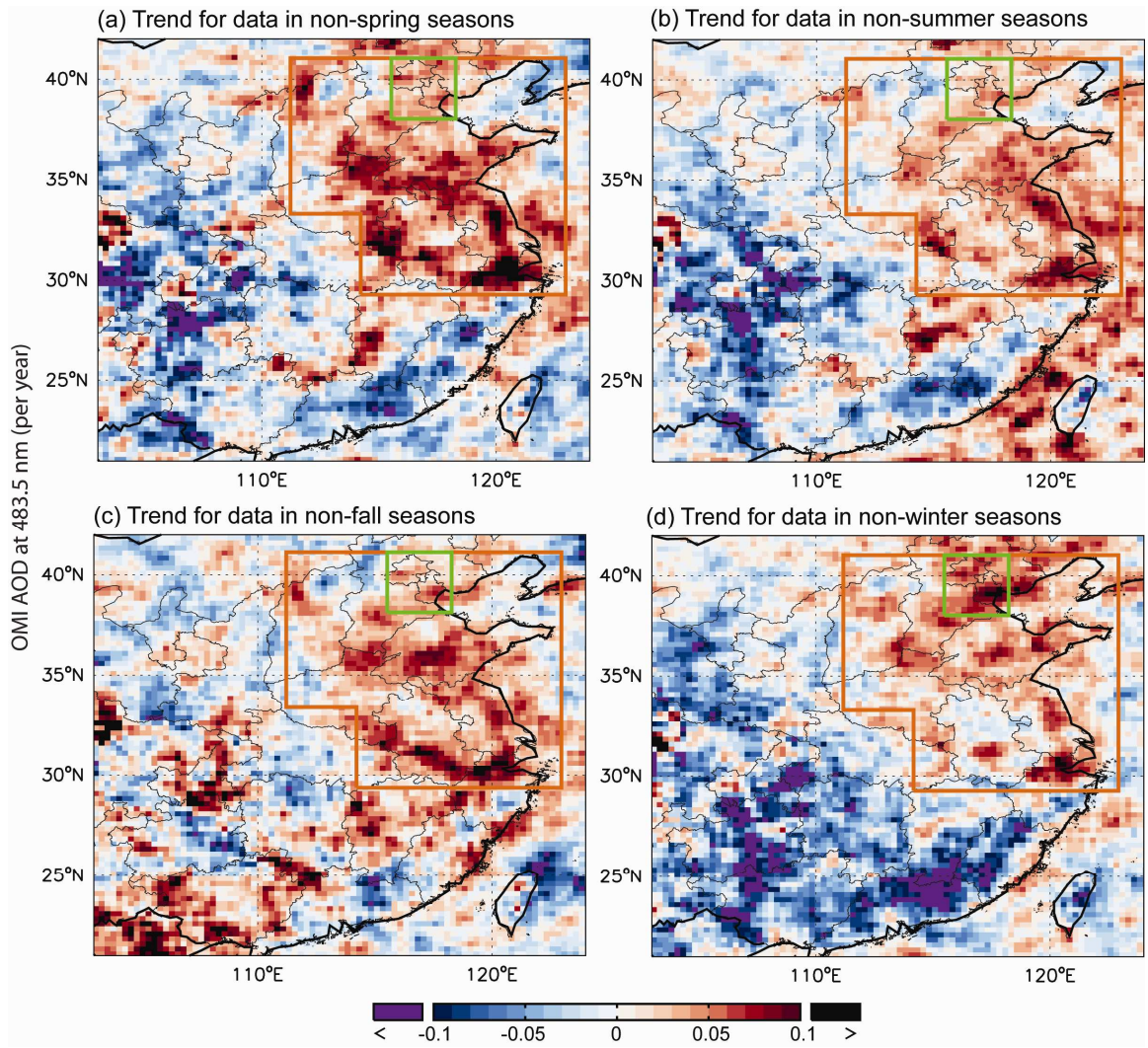


**Figure S7.**

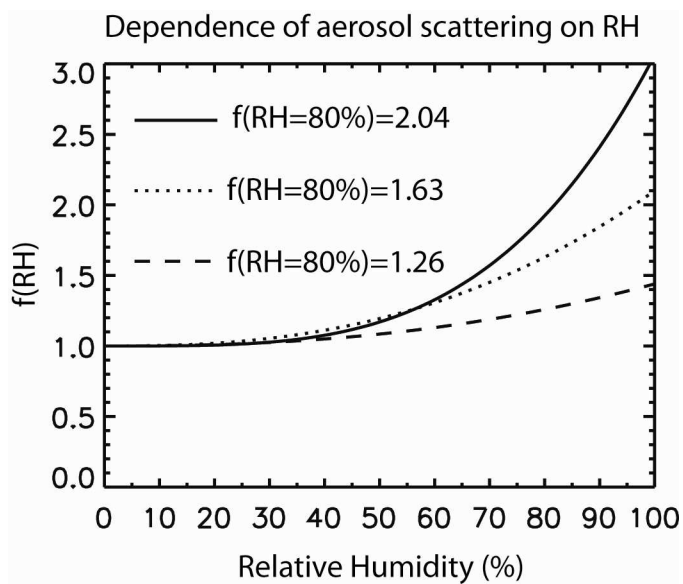


**Figure S8.**

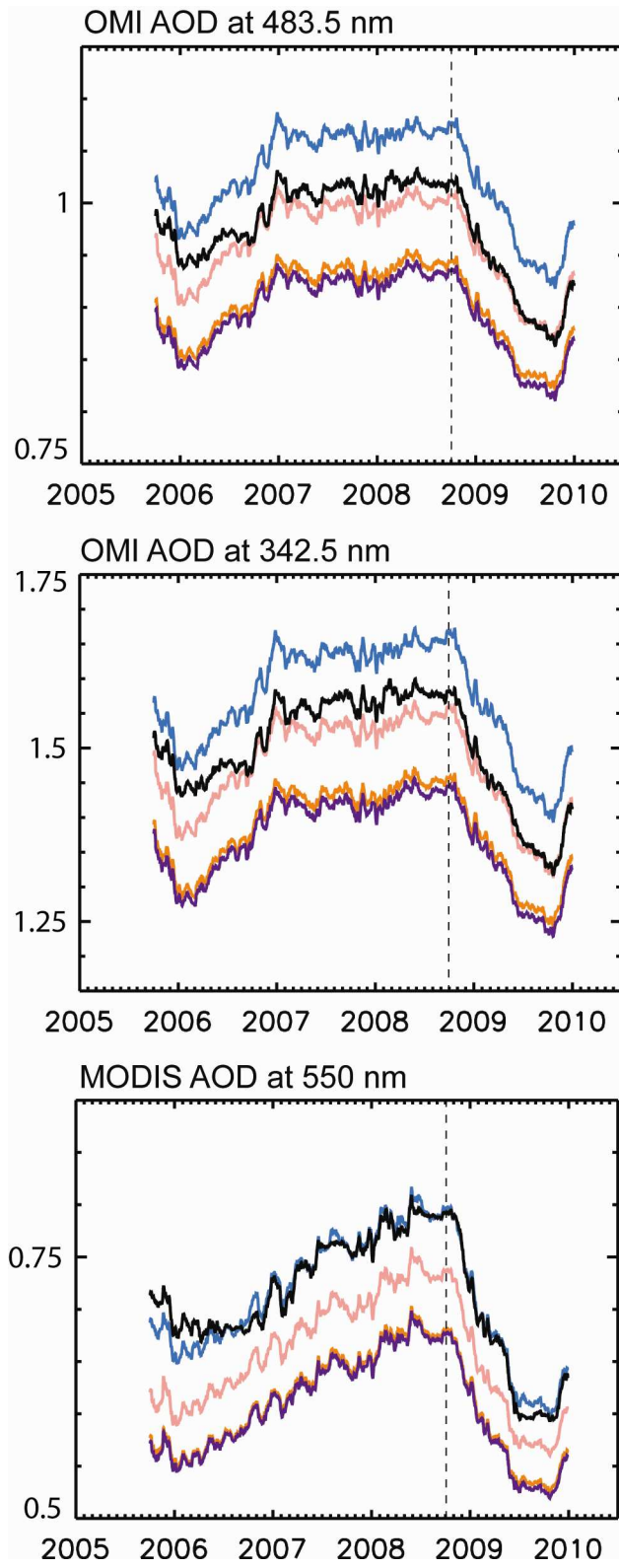


Figure S9.

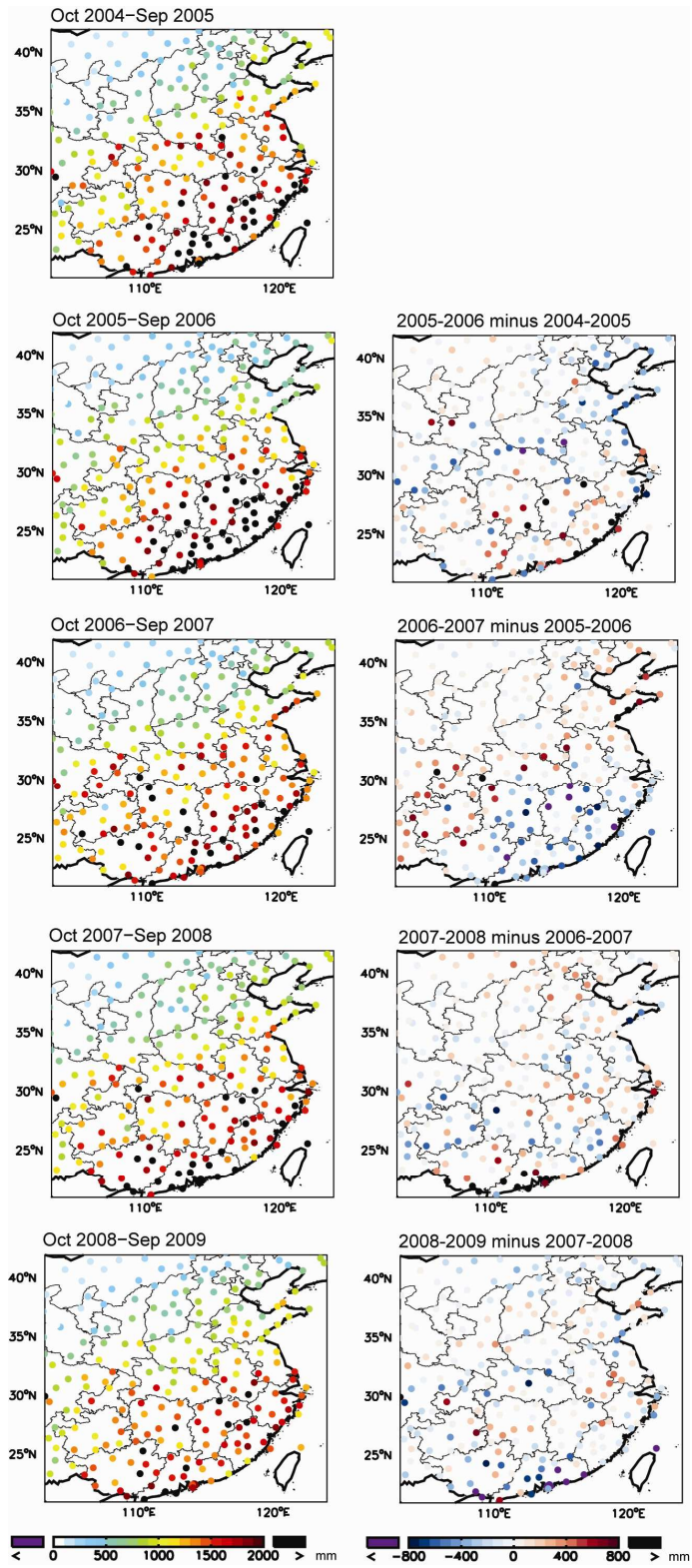


Figure S10.

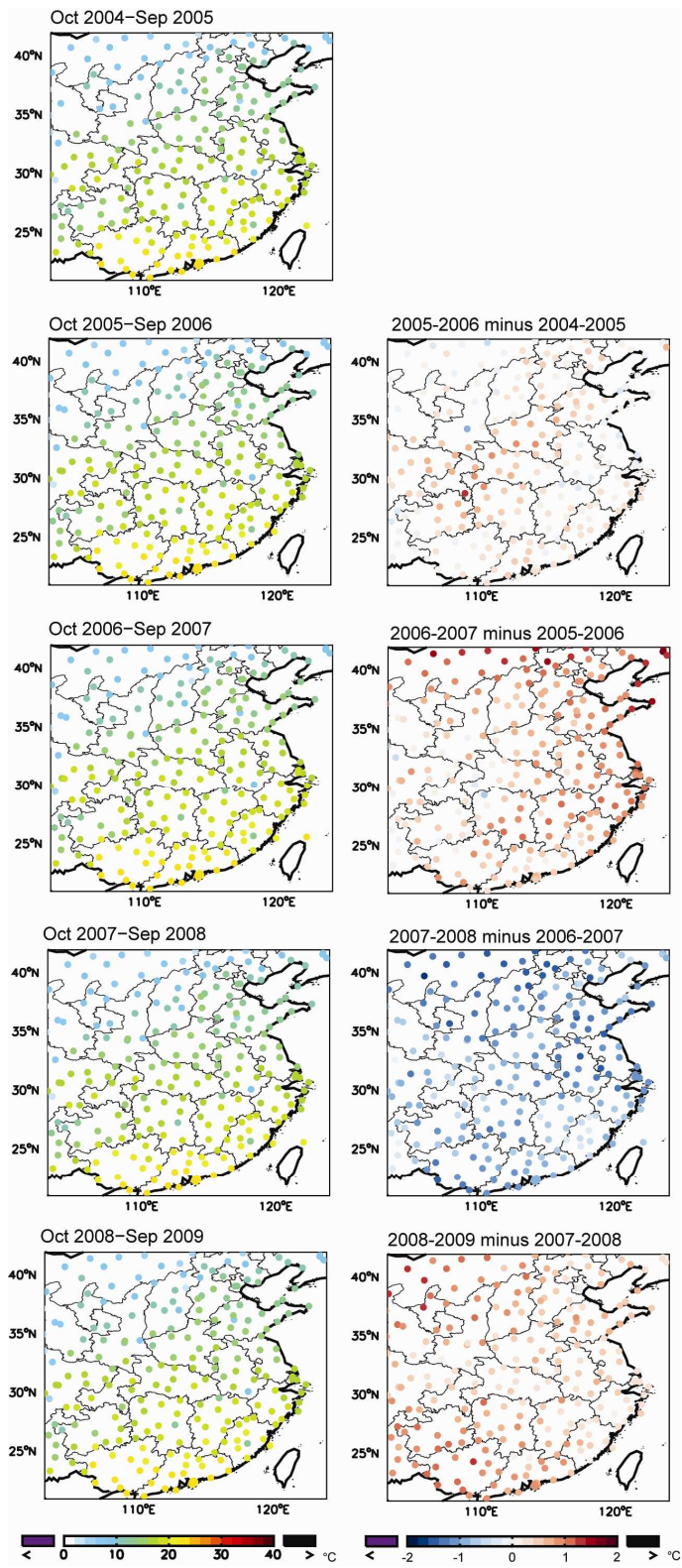


Figure S11.

## References:

- (1) Lei, Y. Research on Anthropogenic Emissions and Control of Primary Particles and Its Key Chemical Components. Tsinghua University, Beijing, China, 2008.
- (2) Lei, Y.; Zhang, Q.; Nielsen, C. P.; He, K., An inventory of primary air pollutants and CO<sub>2</sub> emissions from cement production in China, 1990-2020. *submitted to Atmospheric Environment* **2010**.
- (3) State Environmental Protection Administration (SEPA), Emission Standard of Air Pollutants for Cement Industry: GB4915-2004 (in Chinese). In China Environmental Science Press: Beijing, China, 2004.
- (4) Lei, Y.; He, K.-B.; Zhang, Q.; Liu, Z.-Y., Technology-based Emission Inventory of Particulate Matters (PM) from Cement Industry (in Chinese). *Environmental Science* **2008**, 29, (7), 336-341.
- (5) State Environmental Protection Administration (SEPA), Emission Standard of Air Pollutants for Thermal Power Plants: GB13223-2003 (in Chinese). In China Environmental Science Press: Beijing, China, 2003.
- (6) Zhao, Y.; Wang, S. X.; Duan, L.; Lei, Y.; Cao, P. F.; Hao, J. M., Primary air pollutant emissions of coal-fired power plants in China: Current status and future prediction. *Atmospheric Environment* **2008**, 42, (36), 8442-8452.
- (7) International Energy Agency (IEA), *World Energy Outlook 2007: China and India Insights*. OECD/IEA: Paris, France, 2007; p 663.
- (8) *China Environment Yearbook 1990-2008*. China Environment Yearbook Press: Beijing, China, 1990-2008.
- (9) Zhao, Y.; Duan, L.; Xing, J.; Larssen, T.; Nielsen, C. P.; Hao, J. M., Soil Acidification in China: Is Controlling SO<sub>2</sub> Emissions Enough? *Environmental Science & Technology* **2009**, 43, (21), 8021-8026.
- (10) Zhang, Q.; Streets, D. G.; Carmichael, G. R.; He, K. B.; Huo, H.; Kannari, A.; Klimont, Z.; Park, I. S.; Reddy, S.; Fu, J. S.; Chen, D.; Duan, L.; Lei, Y.; Wang, L. T.; Yao, Z. L., Asian emissions in 2006 for the NASA INTEX-B mission. *Atmospheric Chemistry and Physics* **2009**, 9, (14), 5131-5153.
- (11) Zhao, Y.; Wang, S.; Nielsen, C. P.; Li, X.; Hao, J., Establishment of a database of emission factors for atmospheric pollutants from Chinese coal-fired power plants *Atmospheric Environment in press*, **2010**.
- (12) Wang, M.; Huo, H.; Johnson, L.; He, D. *Projection of Chinese Motor Vehicle Growth, Oil Demand, and CO<sub>2</sub> Emissions through 2050*; Energy Systems Division, Argonne National Laboratory: Argonne, Illinois, 2006; p 70.
- (13) Wei, W. Research and Forecast on Chinese Anthropogenic Emissions of Volatile Organic compounds. Tsinghua University, Beijing, China, 2009.
- (14) *China Statistical Yearbook 2008*. China Statistics Press: Beijing, China, 2008.
- (15) Torres, O.; Decae, R.; Veefkind, J. P.; de Leeuw, G., OMI Aerosol Retrieval Algorithm. In *OMI Algorithm Theoretical Basis Document, vol III, Clouds, Aerosols and Surface UV Irradiance, ATBD-OMI-03*, Stammes, P.; Noordhoek, R., Eds. KNMI: De Bilt, Netherlands, 2002; pp 47-71.

- (16) Torres, O.; Tanskanen, A.; Veihelmann, B.; Ahn, C.; Braak, R.; Bhartia, P. K.; Veefkind, P.; Levelt, P., Aerosols and surface UV products from Ozone Monitoring Instrument observations: An overview. *Journal of Geophysical Research-Atmospheres* **2007**, *112*, (D24).
- (17) README for OMAEROe (OMI Daily L3e for OMAERO). [http://disc.sci.gsfc.nasa.gov/Aura/data-holdings/OMI/documents/v003/OMAEROe\\_OSIPS\\_README\\_V003.doc](http://disc.sci.gsfc.nasa.gov/Aura/data-holdings/OMI/documents/v003/OMAEROe_OSIPS_README_V003.doc)
- (18) Curier, R. L.; Veefkind, J. P.; Braak, R.; Veihelmann, B.; Torres, O.; de Leeuw, G., Retrieval of aerosol optical properties from OMI radiances using a multiwavelength algorithm: Application to western Europe. *Journal of Geophysical Research-Atmospheres* **2008**, *113*, (D17s90).
- (19) Brinksma, E. J.; Pinardi, G.; Volten, H.; Braak, R.; Richter, A.; Schonhardt, A.; van Roozendaal, M.; Fayt, C.; Hermans, C.; Dirksen, R. J.; Vlemmix, T.; Berkhout, A. J. C.; Swart, D. P. J.; Oetjen, H.; Wittrock, F.; Wagner, T.; Ibrahim, O. W.; de Leeuw, G.; Moerman, M.; Curier, R. L.; Celarier, E. A.; Cede, A.; Knap, W. H.; Veefkind, J. P.; Eskes, H. J.; Allaart, M.; Rothe, R.; Pitters, A. J. M.; Levelt, P. F., The 2005 and 2006 DANDELIONS NO<sub>2</sub> and aerosol intercomparison campaigns. *Journal of Geophysical Research-Atmospheres* **2008**, *113*, (D16).
- (20) Livingston, J. M.; Redemann, J.; Russell, P. B.; Torres, O.; Veihelmann, B.; Veefkind, P.; Braak, R.; Smirnov, A.; Remer, L.; Bergstrom, R. W.; Coddington, O.; Schmidt, K. S.; Pilewskie, P.; Johnson, R.; Zhang, Q., Comparison of aerosol optical depths from the Ozone Monitoring Instrument (OMI) on Aura with results from airborne sunphotometry, other space and ground measurements during MILAGRO/INTEX-B. *Atmospheric Chemistry and Physics* **2009**, *9*, (18), 6743-6765.
- (21) Remer, L. A.; Kaufman, Y. J.; Tanre, D.; Mattoo, S.; Chu, D. A.; Martins, J. V.; Li, R. R.; Ichoku, C.; Levy, R. C.; Kleidman, R. G.; Eck, T. F.; Vermote, E.; Holben, B. N., The MODIS aerosol algorithm, products, and validation. *Journal of the Atmospheric Sciences* **2005**, *62*, (4), 947-973.
- (22) Remer, L. A.; Kleidman, R. G.; Levy, R. C.; Kaufman, Y. J.; Tanre, D.; Mattoo, S.; Martins, J. V.; Ichoku, C.; Koren, I.; Yu, H. B.; Holben, B. N., Global aerosol climatology from the MODIS satellite sensors. *Journal of Geophysical Research-Atmospheres* **2008**, *113*, (D14s07).
- (23) Levy, R. C.; Remer, L. A.; Tanré, D.; Mattoo, S.; Kaufman, Y. J. *ALGORITHM FOR REMOTE SENSING OF TROPOSPHERIC AEROSOL OVER DARK TARGETS FROM MODIS: Collections 005 and 051: Revision 2; Feb 2009; 2009; p 96.*
- (24) Choi, Y. S.; Ho, C. H.; Kim, J.; Gong, D. Y.; Park, R. J., The impact of aerosols on the summer rainfall frequency in China. *Journal of Applied Meteorology and Climatology* **2008**, *47*, (6), 1802-1813.
- (25) Gong, D. Y.; Ho, C. H.; Chen, D. L.; Qian, Y.; Choi, Y. S.; Kim, J. W., Weekly cycle of aerosol-meteorology interaction over China. *Journal of Geophysical Research-Atmospheres* **2007**, *112*, (D22202).
- (26) Zhou, K.; Ye, Y. H.; Liu, Q.; Liu, A. J.; Peng, S. L., Evaluation of ambient air quality in Guangzhou, China. *Journal of Environmental Sciences-China* **2007**, *19*, (4), 432-437.

- (27) Choi, Y. S.; Ho, C. H.; Chen, D.; Noh, Y. H.; Song, C. K., Spectral analysis of weekly variation in PM10 mass concentration and meteorological conditions over China. *Atmospheric Environment* **2008**, *42*, (4), 655-666.
- (28) Choi, Y. S.; Park, R. J.; Ho, C. H., Estimates of ground-level aerosol mass concentrations using a chemical transport model with Moderate Resolution Imaging Spectroradiometer (MODIS) aerosol observations over East Asia. *Journal of Geophysical Research-Atmospheres* **2009**, *114*, D04204.
- (29) Li, Z. Q.; Niu, F.; Lee, K. H.; Xin, J. Y.; Hao, W. M.; Nordgren, B.; Wang, Y. S.; Wang, P. C., Validation and understanding of moderate resolution imaging spectroradiometer aerosol products (C5) using ground-based measurements from the handheld Sun photometer network in China. *Journal of Geophysical Research-Atmospheres* **2007**, *112*, (D22s07).
- (30) Xia, X. G.; Li, Z. Q.; Holben, B.; Wang, P.; Eck, T.; Chen, H. B.; Cribb, M.; Zhao, Y. X., Aerosol optical properties and radiative effects in the Yangtze Delta region of China. *Journal of Geophysical Research-Atmospheres* **2007**, *112*, (D22S12).
- (31) Li, Z. Q.; Chen, H.; Cribb, M.; Dickerson, R.; Holben, B.; Li, C.; Lu, D.; Luo, Y.; Maring, H.; Shi, G.; Tsay, S. C.; Wang, P.; Wang, Y.; Xia, X.; Zheng, Y.; Yuan, T.; Zhao, F., Preface to special section on east Asian studies of tropospheric aerosols: An international regional experiment (EAST-AIRE). *Journal of Geophysical Research-Atmospheres* **2007**, *112*, (D22s00).
- (32) Boersma, K. F.; Eskes, H. J.; Veefkind, J. P.; Brinksma, E. J.; van der A, R. J.; Sneep, M.; van den Oord, G. H. J.; Levelt, P. F.; Stammes, P.; Gleason, J. F.; Bucsela, E. J., Near-real time retrieval of tropospheric NO<sub>2</sub> from OMI. *Atmospheric Chemistry and Physics* **2007**, *7*, (8), 2103-2118.
- (33) Boersma, K. F.; Jacob, D. J.; Bucsela, E. J.; Perring, A. E.; Dirksen, R.; van der A, R. J.; Yantosca, R. M.; Park, R. J.; Wenig, M. O.; Bertram, T. H.; Cohen, R. C., Validation of OMI tropospheric NO<sub>2</sub> observations during INTEX-B and application to constrain NO<sub>x</sub> emissions over the eastern United States and Mexico. *Atmospheric Environment* **2008**, *42*, (19), 4480-4497.
- (34) Boersma, K. F.; Jacob, D. J.; Trainic, M.; Rudich, Y.; DeSmedt, I.; Dirksen, R.; Eskes, H. J., Validation of urban NO<sub>2</sub> concentrations and their diurnal and seasonal variations observed from the SCIAMACHY and OMI sensors using in situ surface measurements in Israeli cities. *Atmospheric Chemistry and Physics* **2009**, *9*, (12), 3867-3879.
- (35) Seinfeld, J. H.; Carmichael, G. R.; Arimoto, R.; Conant, W. C.; Brechtel, F. J.; Bates, T. S.; Cahill, T. A.; Clarke, A. D.; Doherty, S. J.; Flatau, P. J.; Huebert, B. J.; Kim, J.; Markowicz, K. M.; Quinn, P. K.; Russell, L. M.; Russell, P. B.; Shimizu, A.; Shinzuka, Y.; Song, C. H.; Tang, Y. H.; Uno, I.; Vogelmann, A. M.; Weber, R. J.; Woo, J. H.; Zhang, X. Y., ACE-ASIA - Regional climatic and atmospheric chemical effects of Asian dust and pollution. *Bulletin of the American Meteorological Society* **2004**, *85*, (3), 367-380.
- (36) Liu, X. G.; Cheng, Y. F.; Zhang, Y. H.; Jung, J. S.; Sugimoto, N.; Chang, S. Y.; Kim, Y. J.; Fan, S. J.; Zeng, L. M., Influences of relative humidity and particle chemical composition on aerosol scattering properties during the 2006 PRD campaign. *Atmospheric Environment* **2008**, *42*, (7), 1525-1536.

- (37) Liu, X. G.; Zhang, Y. H.; Jung, J. S.; Gu, J. W.; Li, Y. P.; Guo, S.; Chang, S. Y.; Yue, D. L.; Lin, P.; Kim, Y. J.; Hu, M.; Zeng, L. M.; Zhu, T., Research on the hygroscopic properties of aerosols by measurement and modeling during CAREBeijing-2006. *Journal of Geophysical Research-Atmospheres* **2009**, *114*, D00g16.
- (38) Yan, P.; Pan, X. L.; Tang, J.; Zhou, X. J.; Zhang, R. J.; Zeng, L. M., Hygroscopic growth of aerosol scattering coefficient: A comparative analysis between urban and suburban sites at winter in Beijing. *Particuology* **2009**, *7*, (1), 52-60.
- (39) Xu, J.; Bergin, M. H.; Yu, X.; Liu, G.; Zhao, J.; Carrico, C. M.; Baumann, K., Measurement of aerosol chemical, physical and radiative properties in the Yangtze delta region of China. *Atmospheric Environment* **2002**, *36*, (2), 161-173.
- (40) Drury, E.; Jacob, D. J.; Spurr, R. J. D.; Wang, J.; Shinozuka, Y.; Anderson, B.; Clarke, A.; Dibb, J.; McNaughton, C.; Weber, R., Synthesis of satellite (MODIS), aircraft (ICARTT), and surface (IMPROVE, EPA-AQS, AERONET) aerosol observations over eastern North America to improve MODIS aerosol retrievals and constrain surface aerosol concentrations and sources. *Journal of Geophysical Research in press*, **2010**.
- (41) Streets, D. G.; Bond, T. C.; Carmichael, G. R.; Fernandes, S. D.; Fu, Q.; He, D.; Klimont, Z.; Nelson, S. M.; Tsai, N. Y.; Wang, M. Q.; Woo, J. H.; Yarber, K. F., An inventory of gaseous and primary aerosol emissions in Asia in the year 2000. *Journal of Geophysical Research-Atmospheres* **2003**, *108*, (D21), 8809.
- (42) Zhang, Q.; Streets, D. G.; He, K.; Wang, Y.; Richter, A.; Burrows, J. P.; Uno, I.; Jang, C. J.; Chen, D.; Yao, Z.; Lei, Y., NO<sub>x</sub> emission trends for China, 1995–2004: The view from the ground and the view from space. *J. Geophys. Res.* **2007**, *112*, (D22306).